11-2019

Pharmacokinetics of ^{99m}Tc-HMPAO in Isolated Perfused Rat Lungs

Anne V. Clough
Marquette University, anne.clough@marquette.edu

Katherine Barry
Marquette University

Benjamin Michael Rizzo
Marquette University, benjamin.rizzo@marquette.edu

Elizabeth R. Jacobs
Medical College of Wisconsin

Said H. Audi
Marquette University, said.audi@marquette.edu

Journal of Applied Physiology, Vol. 127, No. 5 (November 2019): 1317-1327. DOI.

Pharmacokinetics of ^{99m}Tc-HMPAO in Isolated Perfused Rat Lungs

Anne V. Clough
Department of Mathematics, Statistics, and Computer Science, Marquette University, Milwaukee, Wisconsin
Milwaukee Veterans Affairs Medical Center, Milwaukee, Wisconsin
Katherine Barry
Department of Biomedical Engineering, Marquette University, Milwaukee, Wisconsin
Benjamin M. Rizzo
Department of Mathematics, Statistics, and Computer Science, Marquette University, Milwaukee, Wisconsin
Elizabeth R. Jacobs
Milwaukee Veterans Affairs Medical Center, Milwaukee, Wisconsin
Department of Medicine, Medical College of Wisconsin, Milwaukee, Wisconsin
Said H. Audi
Milwaukee Veterans Affairs Medical Center, Milwaukee, Wisconsin

Department of Biomedical Engineering, Marquette University, Milwaukee, Wisconsin

Abstract

Lung uptake of technetium-labeled hexamethylpropyleneamine oxime (HMPAO) increases in rat models of human acute lung injury, consistent with increases in lung tissue glutathione (GSH). Since ^{99m}Tc-HMPAO uptake is the net result of multiple cellular and vascular processes, the objective was to develop an approach to investigate the pharmacokinetics of ^{99m}Tc-HMPAO uptake in isolated perfused rat lungs. Lungs of anesthetized rats were excised and connected to a ventilation-perfusion system. ^{99m}Tc-HMPAO (56 MBq) was injected into the pulmonary arterial cannula, a time sequence of images was acquired, and lung time-activity curves were constructed. Imaging was repeated with a range of pump flows and perfusate albumin concentrations and before and after depletion of GSH with diethyl maleate (DEM). A pharmacokinetic model of ^{99m}Tc-HMPAO pulmonary disposition was developed and used for quantitative interpretation of the time-activity curves. Experimental results reveal that ^{99m}Tc-HMPAO lung uptake, defined as the steady-state value of the ^{99m}Tc-HMPAO lung time-activity curve, was inversely related to pump flow. Also, ^{99m}Tc-HMPAO lung uptake decreased by ~65% after addition of DEM to the perfusate. Increased perfusate albumin concentration also resulted in decreased ^{99m}Tc-HMPAO lung uptake. Model simulations under in vivo flow conditions indicate that lung tissue GSH is the dominant factor in ^{99m}Tc-HMPAO retention in lung tissue. The approach allows for evaluation of the dominant factors that determine imaging biomarker uptake, separation of the contributions of pulmonary versus systemic processes, and application of this knowledge to in vivo studies.

NEW & NOTEWORTHY We developed an approach for studying the pharmacokinetics of technetium-labeled hexamethylpropyleneamine oxime (^{99m}Tc-HMPAO) in isolated perfused lungs. A distributed-in-space-and-time computational model was fit to data and used to investigate questions that cannot readily be addressed in vivo. Experimental and modeling results indicate that tissue GSH is the dominant factor in ^{99m}Tc-HMPAO retention in lung tissue. This modeling approach can be readily extended to investigate the lung pharmacokinetics of other biomarkers and models of lung injury and treatment thereof.

INTRODUCTION

Technetium-labeled hexamethylpropyleneamine oxime (^{99m}Tc-HMPAO) is a radiolabeled compound used in clinical single-photon emission tomography (SPECT) brain perfusion imaging because of its prolonged flow-dependent retention (17). In addition, increased ^{99m}Tc-HMPAO lung uptake has been reported in patients with lung injury resulting from chemotherapy and radiation injury in the absence of perfusion impairment or roentgenographic abnormalities (25) and in patients with diffuse infiltrative lung disease (13). Also, we and others have reported the potential utility of ^{99m}Tc-HMPAO imaging for detecting and monitoring lung injury in preclinical models involving prolonged exposure to high concentrations of oxygen (hyperoxia) (4, 5, 10), the sepsis mimic lipopolysaccharide (6), and chemotoxic agents (12). These studies revealed increased lung uptake in subjects with subclinical lung injury, suggesting that ^{99m}Tc-HMPAO imaging may be a means for quantitatively detecting lung injury before detection with conventional clinical tools and for assessing the efficacy of novel therapies (5).

HMPAO exists in two forms: the oxidized cell-permeant form and the reduced cell-impermeant form (20). The oxidized form is highly lipophilic, with an octanol-water partition coefficient of ~83, compared with 0.006 for the reduced form (2). Thus ^{99m}Tc-HMPAO uptake is dependent on the rate of diffusion of the oxidized form across the cell membrane, where once across the cell membrane it is converted to its reduced cell-impermeant form and retained within the tissue or diffuses back to the blood. The intracellular conversion and retention of HMPAO are dependent in part on the oxidoreductive state of the tissue including the intracellular content of the antioxidant glutathione (GSH) (4, 20).

Lung tissue GSH content increases in response to oxidative stress, which plays a key role in the pathogenesis of lung diseases, including acute lung injury (16, 21). We and others have demonstrated that the lung uptake of HMPAO is dependent on lung tissue GSH content (4–6) and hence can serve as a biomarker of lung tissue GSH content. However, lung uptake of ^{99m}Tc-HMPAO is the net result of multiple cellular and vascular processes, including cardiac output, plasma and tissue GSH content, plasma protein binding, uptake by other organs, capillary endothelial permeability, and mitochondrial and/or cytosolic redox status (1, 17, 19, 20). Each of these cellular and vascular processes, most of which cannot be assessed in vivo, can vary with acute illness. Thus clinical use of ^{99m}Tc-HMPAO for assessing lung pathology necessitates knowledge of the sensitivity and specificity of uptake to changes in the targeted lung cellular process (i.e., GSH content) induced by the disease pathology versus alteration of some other process(es) (e.g., cardiac output, vascular permeability, input function) (4, 17).

The objective of this study was to use ^{99m}Tc-HMPAO imaging of an isolated perfused lung (IPL) to readily and knowingly manipulate the vascular and tissue processes hypothesized to determine ^{99m}Tc-HMPAO lung uptake. The pharmacokinetics of ^{99m}Tc-HMPAO uptake in the lung were investigated via experimental studies, and a physiologically based pharmacokinetic (PBPK) model (8, 9) descriptive of ^{99m}Tc-HMPAO disposition in the lung was used to estimate parameters descriptive of the various processes.

There is ample evidence that the lung uptake of ^{99m}Tc-HMPAO is relatively fast on passage through the pulmonary circulation (4, 6, 10). Thus the assumption of well-mixed compartments made by existing models for ^{99m}Tc-HMPAO brain pharmacokinetics (1, 2, 17, 20) may not be appropriate in the lung, especially since lung capillary perfusion is highly heterogeneous, with some pathways having short transit times and other having long transit times (23). Furthermore, the injected bolus contains the oxidized form of ^{99m}Tc-HMPAO, which is highly lipophilic (2). Thus we developed a distributed-in-space-and-time PBPK model for interpretation of the measured lung time-activity curves (TACs).

MATERIALS AND METHODS

HMPAO (Ceretec) was purchased in kit form from GE Healthcare (Arlington Heights, IL). Diethyl maleate (DEM) and other reagent-grade chemicals were purchased from Sigma-Aldrich (St. Louis, MO).

Experimental methods.

This protocol was approved by the Institutional Animal Care and Use Committee of the Department of Veterans Affairs Medical Center (Milwaukee, WI). Adult male Sprague-Dawley rats [352 ± 7 (SE) g, *n* = 11] were anesthetized (pentobarbital sodium, 40–50 mg/kg), the lungs were excised, and the pulmonary artery, pulmonary vein, and trachea were cannulated and connected to a ventilation-perfusion system as previously described (23). The lungs were oriented in the upright position. Krebs-Ringer bicarbonate perfusate with 3% or 5% bovine serum albumin (BSA) was maintained at 37°C (pH = 7.4) (21), and lungs were ventilated at 40 breaths/min (15% O_2, 6% CO_2, balance N_2) with end-inspiratory and end-expiratory airway pressures of ~6 and 3 mmHg, respectively.

A modular gamma camera (4.5 in. × 4.5 in.) attached to a parallel-hole collimator of a micro-SPECT system was oriented vertically (4, 10). The collimator was positioned ~4 cm from the lung to maximize detection efficiency.

HMPAO was conjugated with pertechnetate (TcO_4^-) according to kit directions. Each experiment began with imaging of a calibration phantom (1.7-mL Eppendorf cuvette) containing ~150 MBq of pertechnetate, positioned next to the lung. A bolus of ^{99m}Tc-HMPAO (~56 MBq in 0.2 mL) was loaded into an injection loop with two parallel tubing segments, positioned upstream from the arterial cannula. At end-expiration, the ventilator was stopped and the solenoid valve in the injection loop was activated to divert the lung inflow to the ^{99m}Tc-HMPAO

segment, without changing pressure or flow. Dynamic planar images were acquired every second for 1–2 min (depending on flow) as the ^{99m}Tc-HMPAO bolus perfused the lung in this single-pass system. Ventilation was restored upon completion of the imaging sequence. To evaluate the effect of perfusate flow on ^{99m}Tc-HMPAO uptake, repeated bolus injections and imaging were performed with flows of 5, 10, and 15 mL/min and 3% BSA perfusate. To determine the effect of protein in the perfusate, bolus injections and imaging were performed with perfusate containing either 3% or 5% BSA at a flow of 10 mL/min. To determine the impact of the GSH concentration in the lung, DEM (6 mM) was added to the perfusate reservoir and circulated through the lung for 10 min before ^{99m}Tc-HMPAO bolus injection and imaging.

Image analysis.

For each bolus injection, the time sequence of planar images was analyzed to determine the lung TAC describing ^{99m}Tc-HMPAO lung uptake as a function of time (10). The sum of the time sequence of images was displayed, and a region of interest (ROI) corresponding to the lung was manually outlined with ImageJ. Since knowledge of the input curve to the lung is required for PBPK modeling (24), an ROI was also drawn over the inflow cannula. The resulting ROI masks were then superimposed on the sequence of ^{99m}Tc-HMPAO images and used to calculate TAC curves representing mean counts per pixel within both the lung and input ROIs for each time frame. The preinjection baseline was subtracted from the curve to account for residual ^{99m}Tc-HMPAO from the previous injection, followed by normalization to the injected dose and to the calibration phantom to obtain the TAC in units of mean counts per pixel per second per injected dose for each ROI. Lung uptake was determined as the mean of the lung TAC over the last 5 s of data acquisition, i.e., at steady state.

The image of the calibration phantom was used to calculate the fraction of injected ^{99m}Tc-HMPAO retained in the lung. An ROI was drawn over the image of the phantom, and total counts acquired over 5 s were determined from the phantom ROI. The known activity within the phantom was divided by the ROI counts to determine an image count-to-activity conversion factor. Total counts acquired from the lung image ROI over the last 5 s of imaging were also determined and converted to lung activity with this conversion factor. The fraction of ^{99m}Tc-HMPAO retained in the lung was then calculated as lung activity divided by the known activity injected into the lung.

BSA concentration in perfusate.

The influence of perfusate BSA concentration on the fraction of oxidized ^{99m}Tc-HMPAO bound to BSA was studied with a Centrifree Ultrafiltration Device with Ultracel PL membrane (30,000 NMWL) (Millipore Sigma, St. Louis, MO) as previously described (11). Perfusate solutions with BSA concentrations of 1.5%, 3%, and 5% (pH 7.4) were prepared. For a given concentration, 0.4 mL of ^{99m}Tc-HMPAO (~220 MBq/mL) was added to 1.6 mL of perfusate; 0.1 mL of the mixture was placed in a 1-mL Eppendorf tube (*sample 1*), and another 0.8 mL was transferred to the upper portion of the device. The device was then centrifuged for 3 min (2,000 *g*, 37°C); 0.1 mL of the filtrate was then added to a different Eppendorf tube (*sample 2*). Activity in *samples 1* and *2* was then counted to obtain measures of total (BSA-bound + free) and free ^{99m}Tc-HMPAO in the perfusate.

EXPERIMENTAL RESULTS

Representative image frames acquired during ^{99m}Tc-HMPAO passage through the isolated lung, with pump flow (F) = 10 mL/min and 3% BSA perfusate, are shown in Fig. 1. The corresponding inlet and outlet TACs are shown in Fig. 2. The lung TAC consists of a throughput portion that dominates the early part of the curve and a tissue uptake and retention portion that dominates the later, steady-state portion of the curve. The steady-state portion is consistent with the reduced form being tissue impermeant.

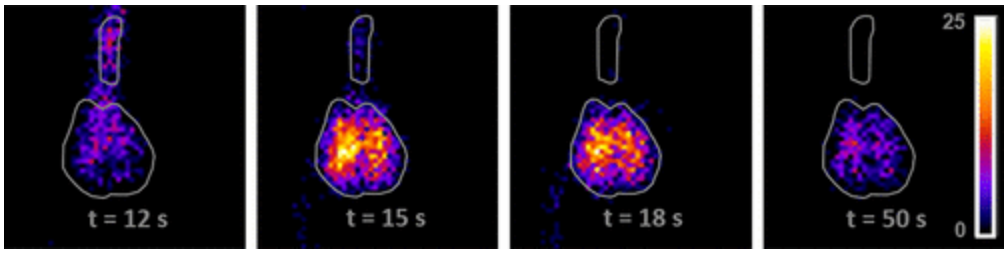

Fig. 1. Representative image frames acquired during ^{99m}Tc-HMPAO passage through an isolated perfused lung showing arterial input and lung regions of interest. Color scale represents counts/s.

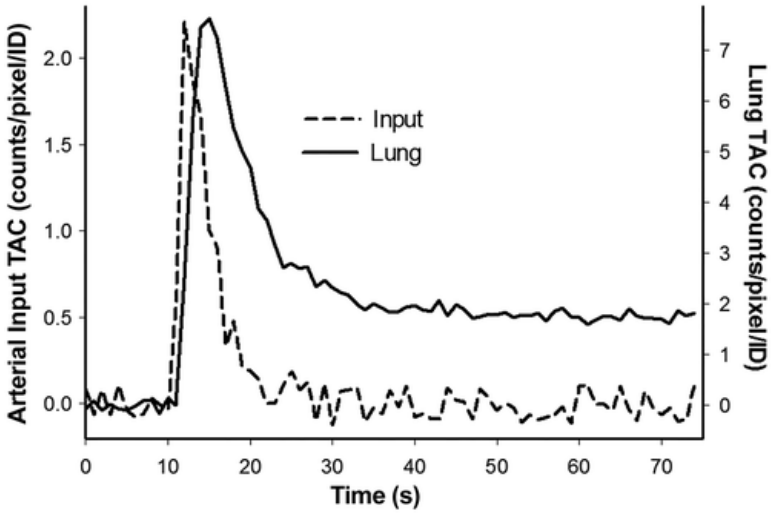

Fig. 2. Representative arterial input and lung time-activity curves (TACs) after bolus injection of ^{99m}Tc-HMPAO with 3% bovine serum albumin perfusate at pump flow = 10 mL/min. Curves normalized to injected dose (ID). *Lefty*-axis is for input; *righty*-axis is for lung.

At F = 10 mL/min with 3% BSA perfusate, 35.9 ± 4.7% (SE; *n* = 8 rats) of the injected dose was retained in the lung tissue during a single pass through the pulmonary circulation, consistent with the relatively high lipophilicity of the oxidized form of ^{99m}Tc-HMPAO.

To determine the effect of flow on lung uptake of ^{99m}Tc-HMPAO, experiments were repeated at F = 5, 10, and 15 mL/min with 3% BSA perfusate. Representative lung TACs shown in Fig. 3*A* show that lung uptake, as measured by the steady-state value of the lung TAC, was inversely related to F. Increasing F from 5 to 10 mL/min resulted in a 36% decrease (paired *t* test, $P < 0.001$) in steady-state lung uptake (4.30 ± 0.30 at 5 mL/min vs. 2.74 ± 0.27 at 10 mL/min, *n* = 8 rats), as shown in Fig. 4. Increasing F to 15 mL/min did not result in a statistically significant decrease in uptake (2.33 ± 0.15, *n* = 5 rats).

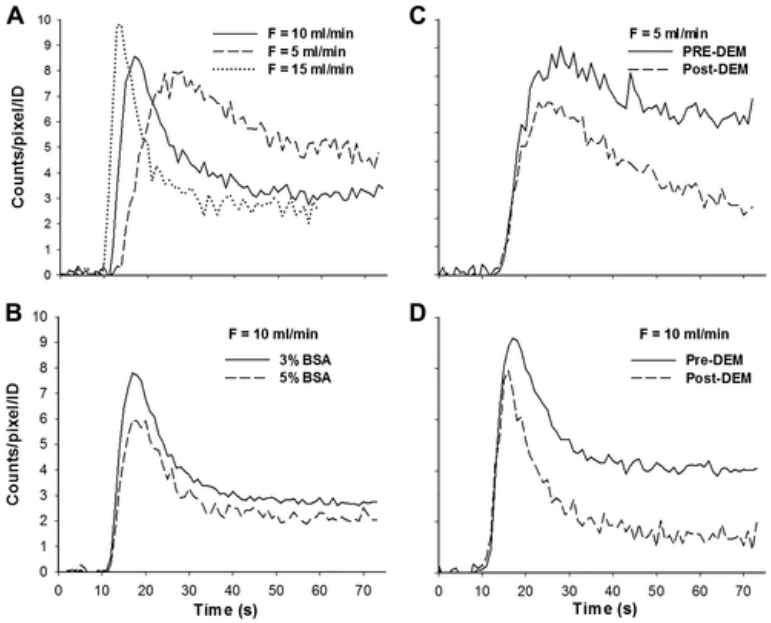

Fig. 3. Representative ^{99m}Tc-HMPAO lung time-activity curves. *A*: pump flow (F) = 5, 10, and 15 mL/min [3% bovine serum albumin (BSA)]. *B*: 3% and 5% BSA perfusate at F = 10 mL/min. *C*: pre- and post-diethyl maleate (DEM) at F = 5 mL/min. *D*: pre- and post-DEM at F = 10 mL/min. Curves normalized to injected dose (ID).

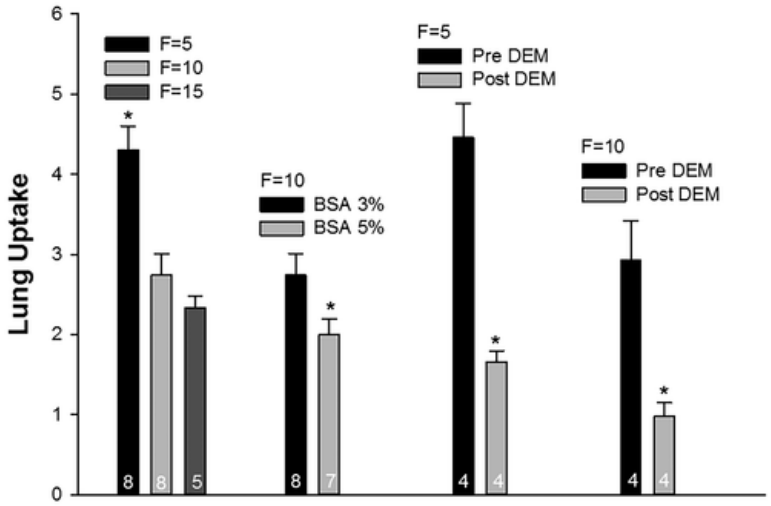

Fig. 4. ^{99m}Tc-HMPAO lung uptake obtained under different experimental conditions, with 3% bovine serum albumin (BSA) unless indicated otherwise. Numbers of rats in groups are indicated in the bars. *P < 0.05 in all cases. DEM, diethyl maleate.

The effect of perfusate BSA concentration on lung uptake of ^{99m}Tc-HMPAO was evaluated with F = 10 mL/min, with resulting TACs shown in Fig. 3*B*. Increasing BSA concentration from 3% (2.74 ± 0.27, n = 8 rats) to 5% (1.92 ± 0.19, n = 7 rats) resulted in a ~30% decrease (P = 0.034, unpaired t test) in lung uptake (Fig. 4). This is consistent with a decrease in the fraction of injected lipophilic ^{99m}Tc-HMPAO available for uptake on passage through the lung with increased BSA concentration.

Figure 5 shows the relationship between perfusate %BSA and the ratio of bound (Bo)-to-free (Fr) ^{99m}Tc-HMPAO in perfusate. The binding reaction

$$\mathrm{Fr} + \mathrm{BSA} \underset{k_{-1}}{\overset{k_1}{\rightleftarrows}} \mathrm{Bo}$$

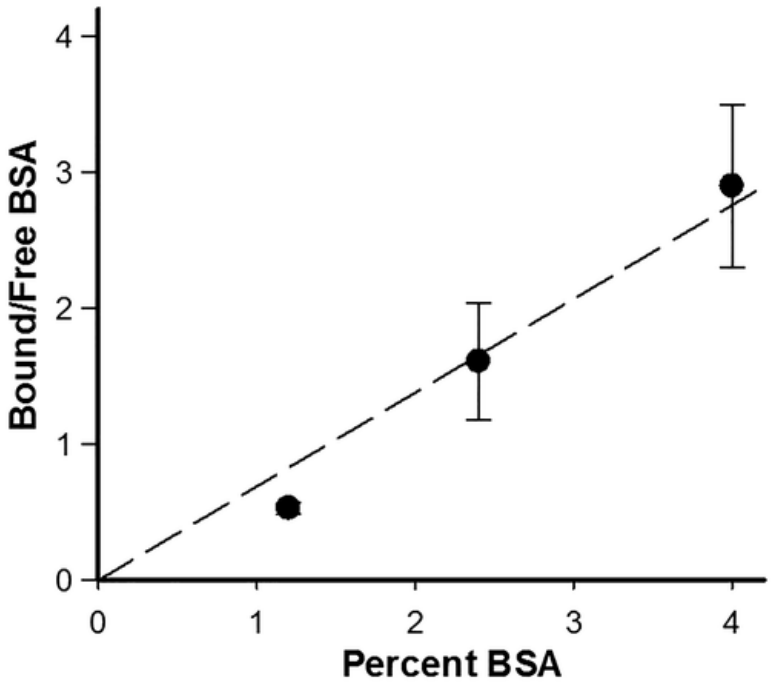

Fig. 5. Ratio of bovine serum albumin (BSA) bound to ^{99m}Tc-HMPAO to free BSA in perfusate as a function of BSA concentration in perfusate. Means ± SD; *n* = 4 rats. $r^2 = 0.84$

under the rapid equilibrium assumption, yields [Fr][BSA]k_1 = [Bo]k_{-1} and hence

$$\frac{[\text{Bo}]}{[\text{Fr}]} = [\text{BSA}]\left(\frac{1}{K_{\text{Dv}}}\right) \quad (1)$$

where K_{Dv} is the equilibrium dissociation constant in units of %BSA. Data in Fig. 5 support this linear relationship, consistent with rapidly binding equilibrium between BSA and ^{99m}Tc-HMPAO. The slope of the regression line through the data yielded an estimated value of K_{Dv} = 1.46%BSA, which was used in the model fitting and simulations below. This result suggests that when perfusate BSA concentration was 3%, ~68% of ^{99m}Tc-HMPAO in perfusate was bound to BSA.

The effect of lung tissue GSH content was evaluated by adding DEM to the perfusate, with representative TACs shown in Fig. 3, *C* and *D*. DEM decreased lung uptake by 62% (4.46 ± 0.42 pre-DEM vs. 1.66 ± 0.14 post-DEM, *n* = 4 rats; paired *t* test, *P* = 0.004) at a flow of 5 mL/min and by 67% (2.93 ± 0.49 pre-DEM vs. 0.98 ± 0.17 post-DEM, *n* = 4 rats; paired *t* test, *P* = 0.009) at 10 mL/min (Fig. 4). These results are consistent with a dominant role for lung tissue GSH content in uptake and retention of ^{99m}Tc-HMPAO on passage through the pulmonary circulation.

PBPK MODEL OF ^{99m}Tc-HMPAO PULMONARY DISPOSITION

Model development.

A distributed-in-time-and-space model (8) was developed and used for quantitative interpretation of the measured lung TACs. The model incorporates the dominant cellular and vascular processes hypothesized to determine the pulmonary disposition of ^{99m}Tc-HMPAO. A system of partial differential equations (PDEs) was constructed that relaxes the assumption of well-mixed compartments and accounts for perfusion heterogeneity within the pulmonary capillary region. The whole organ model then consists of conducting arteries and veins, and capillary elements, each composed of a vascular region and its surrounding extravascular (tissue) region as depicted in Fig. 6. A detailed derivation of the lung model, including the model PDEs, is presented in

the Appendix. Briefly, the injected oxidized form of ^{99m}Tc-HMPAO (O_v) enters the capillary region, where it can participate in rapidly equilibrating interactions with BSA in the perfusate with dissociation rate constant K_{Dv}, diffuse into the extravascular region (PS), or exit the lung. Within the extravascular region, the oxidized form (O_e) converts to the reduced form (R_e) via either a GSH-dependent (k_{GSH}) pathway or other reductant (RH, GSH independent, k_{RH}) pathway that is retained, participates in rapidly equilibrating interactions with protein (dissociation rate constant K_{De}), or diffuses back into the vascular region of the capillaries. The oxidized form in the vasculature exits the capillary region via the conducting veins.

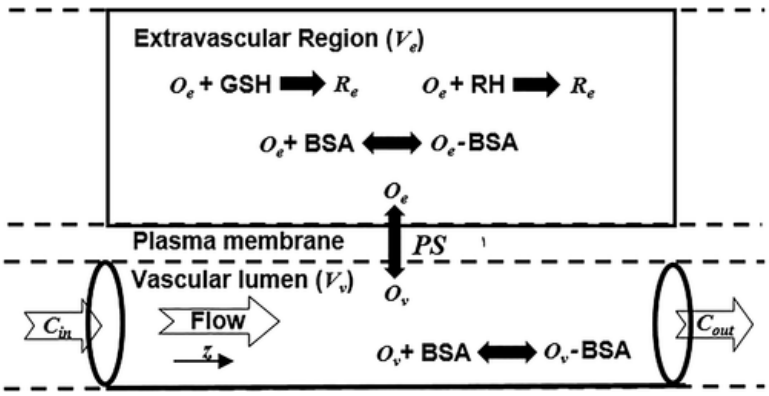

Fig. 6. Model of dominant processes involved in ^{99m}Tc-HMPAO (*O*, oxidized; *R*, reduced) distribution in a single capillary element consisting of vascular (v, blood) and surrounding extravascular (e, cell/tissue) regions. GSH, glutathione; V, volume; *z*, distance from the capillary inlet; RH, GSH-independent reductant; C_{in}, capillary input function; C_{out}, capillary outlet function; PS, permeability surface-area product; BSA, protein.

The resulting PDEs describing the spatial and temporal changes in the concentration of oxidized and reduced ^{99m}Tc-HMPAO in the vascular and extravascular regions of a capillary element derived in the Appendix are given by

$$\frac{\partial \bar{O}_v}{\partial t} + \frac{1}{\mu_c}\frac{\partial \bar{O}_v}{\partial z} = \frac{PS}{V_v}\left(\frac{\bar{O}_v}{1+\frac{P_v}{K_{Dv}}} - \frac{\bar{O}_e}{1+\frac{P_e}{K_{De}}}\right) \quad (2)$$

$$\frac{\partial \bar{O}_e}{\partial t} = \frac{PS}{V_e}\left(\frac{\bar{O}_v}{1+\frac{P_v}{K_{Dv}}} - \frac{\bar{O}_e}{1+\frac{P_e}{K_{De}}}\right) - k_{GSH}\bar{O}_v - k_{RH}\bar{O}_v \quad (3)$$

$$\frac{\partial R_e}{\partial t} = k_{GSH}\bar{O}_v + k_{RH}\bar{O}_v \quad (4)$$

where $\bar{O}_v(z,t)$ is total concentration of free and BSA-bound oxidized ^{99m}Tc-HMPAO in the vascular region at normalized distance *z* from the capillary inlet at time *t*, $\bar{O}_e(z,t)$ is total concentration of free and bound oxidized ^{99m}Tc-HMPAO in the extravascular region, $R_e(z,t)$ is the concentration of reduced ^{99m}Tc-HMPAO in the extravascular region, and the model parameters are defined in Table 1.

Table 1. Model parameters

Unknown Parameters	Definition	Estimated Value
k_{GSH}	GSH-dependent reduction rate constant in extravascular region	0.071 ± 0.030 s^{-1}
k_{RH}	GSH-independent reduction rate constant in extravascular region	0.031 ± 0.005 s^{-1}
PS	Capillary permeability surface area product	125 ± 83 mL/s

$D_e = \frac{P_e}{K_{D_e}}$	Ratio of protein concentration to equilibrium dissociation rate constant for oxidized HMPAO bound to protein in extravascular region	1.12 ± 0.66
Given Parameters	Definition	Fixed Value
V_v	Capillary vascular volume	0.42 mL
V_e	Extravascular tissue volume	1.0 mL
μ_c	Capillary mean transit time	2.5 s
$D_v = \frac{P_v}{K_{D_v}}$	Ratio of BSA perfusate concentration to equilibrium dissociation rate constant for oxidized HMPAO bound to BSA in vascular region	1.06

BSA, bovine serum albumin; GSH, glutathione; HMPAO, hexamethylpropyleneamine oxime.

Equations 2–4 are for a single capillary element. To account for the effect of capillary perfusion kinematics on the lung uptake of ^{99m}Tc-HMPAO, a heterogeneous distribution of pulmonary capillary transit times, $h_c(t)$, was used as described previously (23). $h_c(t)$ was represented with a gamma variate function (18) with mean transit time μ_c = 2.5 s and variance σ_c^2 = 4.0 s^2 at F = 10 mL/min as determined previously (23). The $h_c(t)$ at F = 5 (or 15) mL/min was obtained by rescaling $h_c(t)$ by dividing *t* by 5/10 (or 15/10) and by multiplying its amplitude by 5/10 (or 15/10) (23).

The lung input curve, $C_{art}(t)$, was assumed to take the form of a shifted gamma variate function, which was fit to the experimental lung inlet TAC for each data set. The arterial and venous transit time distributions were each represented by a shifted impulse function with each shift equaling 50% of the noncapillary portion of the lung vascular mean transit time (23). Random coupling conditions were assumed between the arteries and the capillaries, i.e., all capillary elements are exposed to the same capillary input (3, 23).

To reduce computation time, *Eqs. 2–4* for a single capillary element were solved for the capillary with the longest transit time and then subsampled at axial points to obtain individual outflow concentration curves for capillaries with shorter transit times (3, 23). The lung output curve, $C_{vein}(t)$, was then computed as the sum of all capillary outflow curves, each weighted according to $h_c(t)$, and then shifted by the venous transit time. Finally, the model lung time-activity curve describing the total amount of ^{99m}Tc-HMPAO in the lung as a function of time, TAC(*t*), was obtained with

$$\mathrm{TAC}(t) = \mathrm{F}\int_0^t [C_{\mathrm{art}}(t) - C_{\mathrm{vein}}(t)]\,\mathrm{d}t \quad (5)$$

Model fitting results.

Nonlinear regression was used to fit the model solution TAC(*t*) to the experimental lung TACs to obtain estimates of k_{GSH}, k_{RH}, permeability surface area product (PS), and ratio of protein concentration to equilibrium dissociation rate constant for oxidized HMPAO bound to protein in extravascular region (D_e) (Table 1). To reduce correlation between the model parameters, two lung TACs obtained from the same lung, namely pre-DEM and post-DEM at F = 10 mL/min, were fit simultaneously. In this procedure, k_{RH}, PS, and D_e were free parameters but assumed equal for both data sets, whereas k_{GSH} was free for pre-DEM data but set to zero for post-DEM data. This approach is based on the assumption that tissue GSH is depleted after DEM administration. The capillary volume, V_v, was fixed at 0.46 mL (23) whereas the extravascular volume, V_e, was set to 1.0 mL based on lung tissue water volume estimated from lung wet weight and wet-to-dry weight ratio (6). $D_v = P_v/K_{Dv}$ was set to 3/1.46 since experiments were performed with P_v = 3%BSA perfusate and the value obtained above for K_{Dv}. μ_c was set at 2.5 s as indicated above. The model fitting was done in MATLAB with the *lsqcurvefit* function that implemented the trust-region-reflective algorithm, an iterative optimization algorithm that readily incorporates bounds on the values of the parameters. Each model fit was repeated 10 times using randomly generated initial parameter values to avoid trapping in a local minimum solution. The largest difference between final parameter

estimates for all data fits was <0.5%, which provides reasonable confidence that a global minimum was reached in all cases.

A representative result in Fig. 7*A*, obtained at F = 10 mL/min, shows good agreement between the data (points) and the model fit (lines). Figure 8 (pre-DEM Fig. 8, *left*; post-DEM, Fig. 8, *right*) shows the corresponding sensitivity functions that represent the normalized change in the model-fit TAC(*t*) for a 1% change in the value of each free parameter (7). Note that the k_{GSH} and k_{RH} functions have the identical shape and are superimposed for the pre-DEM case, whereas the k_{GSH} function for post-DEM is zero. Each of the others is different from the others, suggesting that pre- and post-DEM lung TACs have sufficient information for estimating the model parameters.

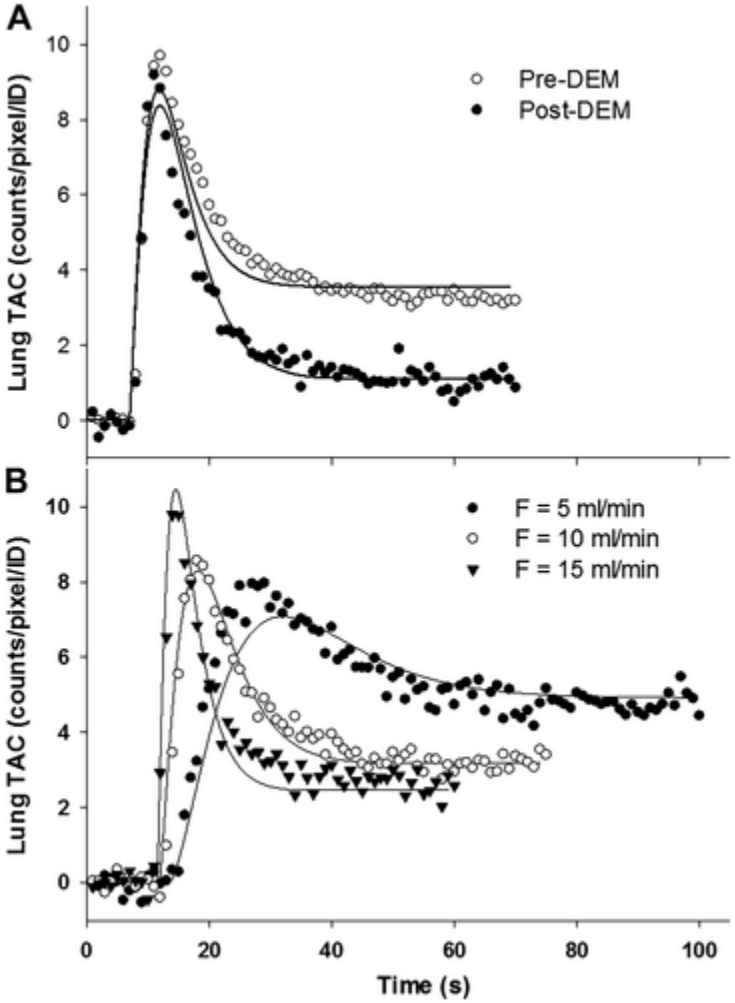

Fig. 7. Representative experimental lung time-activity curves (TACs; points) and simultaneous model fits (lines). *A*: data acquired before (pre-) and after (post-) diethyl maleate (DEM) treatment [pump flow (F) = 10 mL/min]. *B*: data acquired at 3 different flows and model curves obtained with mean ± 1 SD of previously estimated model parameters given in Table 1. ID, injected dose.

Table 2. Baseline model parameters

Model Function or Parameter	Parameter Value
F	100 mL/min
$C_{in}(t)$	μ = 0.24 s; σ² = 0.046 s^2
$h_c(t)$	μ_c = 0.25 s; σ2cσc2 = 0.040 s^2
Arterial transit	μ_a = 0.1 s; σ2aσa2 = 0

Venous transit	μ_v = 0.1 s; σ2vσv2 = 0
BSA concentration	3%
k_{GSH}	0.07 s^{-1}
k_{RH}	0.03 s^{-1}
PS	125 mL/s
D_e	1.1

BSA, bovine serum albumin; $C_{in}(t)$, capillary input function; De, ratio of protein concentration to equilibrium dissociation rate constant for oxidized HMPAO bound to protein in extravascular region; $h_c(t)$, capillary transit time distribution; k_{GSH}, glutathione (GSH)-dependent reduction rate constant; k_{RH}, GSH-independent reduction rate constant; PS, permeability surface area product; μ, mean transit time; σ^2, variance.

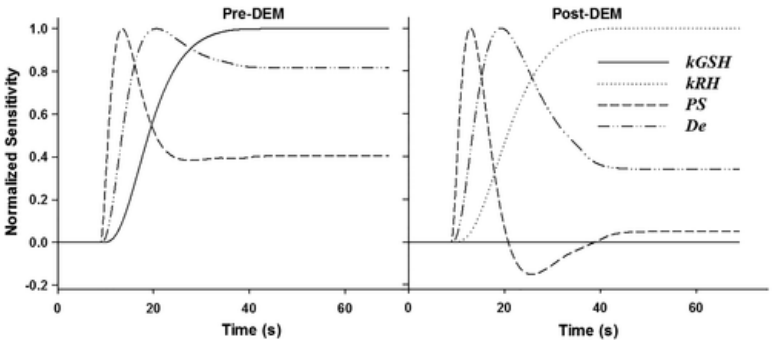

Fig. 8. Model parameter sensitivity functions showing the change in the model solution given a 1% increase in the value of the model parameter. *Left*: pre-diethyl maleate (DEM). *Right*: post-DEM. Each plot is normalized to its maximum value. Parameters given in Table 1.

Table 1 shows the resulting estimated model parameters obtained from four different lungs. The GSH-dependent rate of HMPAO reduction (k_{GSH}) is ~130% larger than that for the GSH-independent rate of HMPAO reduction (k_{RH}), consistent with lung tissue GSH being the dominant factor in HMPAO retention in lung tissue. The estimated value of PS is large compared with the flow range studied, consistent with the oxidized form of HMPAO being highly lipophilic with a large octanol-water partition coefficient.

The model was validated by using it in the forward mode with the estimated parameter values in Table 1 to predict lung TACs. Figure 7*B* shows experimental lung TACs obtained from the same rat lung, but not one used in the summary results of Table 1, at different pump flows together with corresponding model fits. In this case, the model was fit to the three-flow experimental TACs simultaneously while allowing the free model parameters to range within 1 SD of the mean values given in Table 1. Good agreement between the data and the resulting model TAC is observed at all three flows.

The model was also used to predict the resulting lung TACs with a pump flow of 5 mL/min to compare with the corresponding data TACs for the four rat lungs used in Table 1. The mean of the last five data points of each TAC was compared to the steady-state value of the predicted TAC, yielding a relative error of −3.8 ± 6.0 (SD) % in the lung uptake values.

Similarly, the model was used to predict the resulting lung TACs with 3% and 5% BSA concentration, F = 10 mL/min, and the mean estimated parameters in Table 1. The resulting model steady-state values were 2.86 and 2.00 for 3% and 5%, respectively, compared with 2.74 ± 0.27 and 1.92 ± 0.19, respectively for the data values in Fig. 4, a difference of <5% in both cases. This result provides additional support for the model assumption of rapidly equilibrating interactions between ^{99m}Tc-HMPAO and perfusate BSA.

Simulation results.

Simulations were performed to address questions pertinent to in vivo conditions that cannot be readily answered experimentally. A flow of 100 mL/min, corresponding to resting cardiac output of an adult male 350-g Sprague-Dawley rat (15), was used to determine the effect of the key model parameters on steady-state lung uptake. The baseline simulation was performed with model parameters in Table 2, which were rescaled from experiments performed with F = 10 mL/min or obtained from previous studies (23).

Acute lung injury is often accompanied by substantial changes in cardiac output and blood pressure in patients, especially when accompanied with vital mechanical ventilation (20). Simulations were performed in which the flow rate through the lung was set at 50, 100, or 150 mL/min, while the volume of each vascular component was held constant. The steady-state values of the simulated lung TACs were determined and normalized to the F = 100 mL/min baseline case. Results in Fig. 9 show that steady-state lung uptake is inversely related to F, in that a 50% decrease in F resulted in a ~13% increase in lung uptake, whereas a 50% increase in F resulted in a ~8% decrease. This is expected since decreased F allows longer capillary residence times and hence increased uptake.

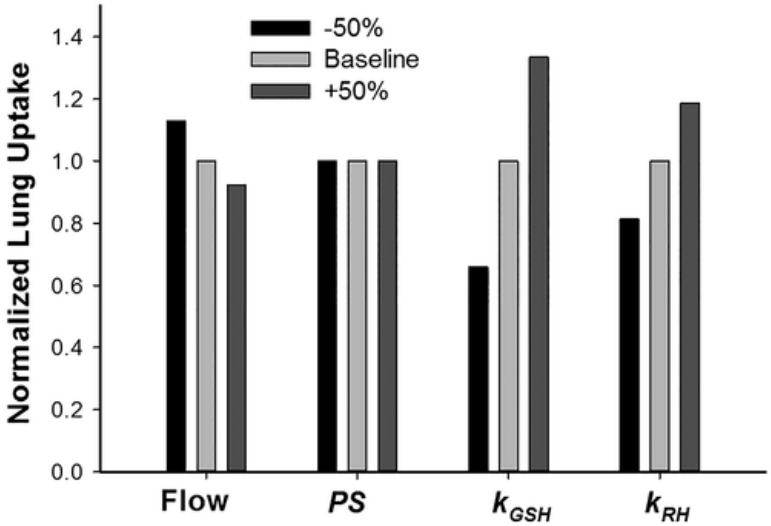

Fig. 9. Lung uptake normalized to baseline case simulated with pump flow = 100 mL/min and parameters given in Table 2. Each parameter was increased or decreased by 50%.

Previous studies have shown that in a hyperoxic model of acute lung injury vascular endothelial permeability is increased by more than ~200% (6). Figure 9 shows that in simulations when PS was varied by ±50%, steady-state lung uptake changed by <1%. Because the estimated value of PS is so large, these flow changes have no measurable effect on the steady-state value of ^{99m}Tc-HMPAO uptake, which is consistent with the sensitivity functions of Fig. 8.

Since previous studies have demonstrated that tissue GSH content plays a key role in ^{99m}Tc-HMPAO retention (4–6, 20), simulations were performed in which k_{GSH} was changed. Figure 9 shows that steady-state uptake increases with k_{GSH}, consistent with more intracellular HMPAO reduction and retention.

Data in Fig. 3, *C* and *D*, suggest an alternate pathway for ^{99m}Tc-HMPAO conversion since there is substantial uptake even when GSH is depleted in the lung after DEM treatment. Although specific pathways have not been clearly identified, there is evidence that mitochondrial dysfunction and/or endothelial amine metabolism dysfunction may be contributors (4). To investigate the contribution of a GSH-independent process, simulations were performed with k_{RH} changed by ±50%. The resulting steady-state values (Fig. 9) increased with increasing k_{RH}, although the changes were smaller than those resulting from corresponding changes in k_{GSH}.

DISCUSSION

An experimental and computational approach for mechanistic and quantitative evaluation of the pharmacokinetics of ^{99m}Tc-HMPAO in the rat IPL was developed. The approach allows for evaluation of the dominant factors that determine lung uptake of ^{99m}Tc-HMPAO and for separation of the contributions of pulmonary processes from systemic processes.

The model accounts for spatial and temporal variations in the concentration of ^{99m}Tc-HMPAO on passage through the pulmonary capillaries. The model relaxes the assumption of well-mixed compartments made in models of ^{99m}Tc-HMPAO pharmacokinetics in other organs. The results of the model simulations demonstrate the utility of ^{99m}Tc-HMPAO for probing tissue GSH content in intact functioning lungs and in vivo.

Sepsis, a leading cause of acute lung injury, often causes lower and variable cardiac output and blood pressure in patients and frequently requires mechanical ventilation (22). Moreover, serum albumin can drop by half in <24 h. Data here reveal that such changes could affect lung uptake of ^{99m}Tc-HMPAO independent of a change in lung tissue GSH content.

In the experiments presented, increasing flow from 5 to 10 mL/min, but not 10 to 15 mL/min, resulted in a significant decrease in steady-state ^{99m}Tc-HMPAO lung uptake (Fig. 4). The pulmonary vasculature consists of distensible blood vessels whose diameters and hence volumes are dependent on the intravascular pressure. Previous studies using this IPL preparation showed that the microvascular pressure [(arterial pressure + venous pressure)/2] increases from ~3 torr to ~4 torr when flow is increased from 10 to 15 mL/min (23). This increase in intravascular pressure results in a ~6% increase in pulmonary vascular volume (14), which is offset by the 50% increase in flow, leading to a smaller overall decrease in lung vascular mean transit time. This increase in volume that occurs with increased flow may explain the relatively small decrease in ^{99m}Tc-HMPAO lung uptake as flow was increased from 10 mL/min to 15 mL/min in the experiments. This effect of flow-induced changes in microvascular pressure on lung vascular volume could be mitigated in the IPL experiments by adjusting the venous pressure to minimize the change in microvascular pressure as pump flow is changed.

Experimental results show that before the addition of DEM 32 ± 4% of the injected ^{99m}Tc-HMPAO was taken up and retained in the isolated lung at a flow of 10 mL/min, whereas after DEM this was decreased to 14 ± 4%. The pre-DEM fraction is much larger than the 7.4% lung retention in vivo reported by Neirinckx et al. (20). This difference is largely due to the large difference between the pump flow (10 mL/min) and the much higher resting cardiac output of an adult Sprague-Dawley rat (~100 mL/min) (15). In this case ^{99m}Tc-HMPAO lung uptake predicted by the model using the parameters in Table 1 is ~6%, providing additional validation of the model.

In the IPL studies here, and the corresponding model, there was no GSH in the perfusate. The presence of GSH in blood plasma (~20 μM) would partially reduce ^{99m}Tc-HMPAO and hence decrease the fraction of the oxidized form of ^{99m}Tc-HMPAO entering the lungs. At a flow of 100 mL/min, model simulations showed that decreasing the fraction of oxidized ^{99m}Tc-HMPAO entering the lungs by 10%, 20%, or 30% decreased steady-state lung uptake by a corresponding ~10%, 20%, and 30%.

There is strong evidence that oxidative stress plays an important role in the early stages of acute respiratory distress syndrome (22), yet there are no good biomarkers for detection of injury before evidence of clinical respiratory distress or infiltrates on computed tomography imaging. Unlike prior markers of lung injury that target changes in pulmonary endothelial permeability, which is altered later in the disease progression, GSH tissue content and the corresponding increase in lung ^{99m}Tc-HMPAO uptake occur early in the disease process (6). In addition, our investigation of ^{99m}Tc-HMPAO is motivated by its status as a clinically approved SPECT radiopharmaceutical in routine use.

The proposed experimental and modeling approach could be readily modified for evaluating key cellular processes in other lung injury models by incorporating appropriate differential equations accounting for those processes into the computational model. Also, the approach could be used directly to investigate changes in the key model parameters that occur with lung injury and hence assess the efficacy of therapeutic treatments thereof. The model could also be modified to quantify uptake of other biomarkers in the lung or other organs (e.g., heart) or for analyzing data from other functional imaging modalities (e.g., MRI, PET). Moreover, the approach can be extended to a whole body model to assess the impact of systemic circulation on the lung uptake of HMPAO.

Model simulations performed at normal cardiac output for a rat indicated that the dominant process in steady-state uptake of ^{99m}Tc-HMPAO was GSH dependent (Fig. 9). To a lesser extent, flow played a role, but that only became apparent when flow was changed by 50%. Changes in PS, which might be expected as a result of vascular injury, had no effect on uptake, presumably because of the high lipophilicity of the oxidized form of ^{99m}Tc-HMPAO. These results have important implications for in vivo preclinical studies and potential clinical use of ^{99m}Tc-HMPAO where presumably only one time-averaged SPECT image volume would be acquired ~30 min after injection. Any observed increase in ^{99m}Tc-HMPAO in the lungs could, with fair confidence, be attributed to an increase in a GSH-dependent process likely involved with lung injury rather than to changes in microvascular permeability or some other process. Changes in cardiac output that may occur in patients could be measured and accounted for in the interpretation of ^{99m}Tc-HMPAO data. Thus the modeling in these preclinical studies is an important step toward that clinical use.

We developed an approach for studying the pharmacokinetics of a clinical SPECT biomarker, ^{99m}Tc-HMPAO, in IPL. Experimental and modeling results indicate that tissue GSH is the dominant factor in ^{99m}Tc-HMPAO retention in lung tissue. This approach allows investigation of questions that cannot readily be addressed in either in vivo preclinical or clinical studies. The MATLAB code for the computational model is available for download at the model sharing website https://www.physiome.org or upon request to the corresponding author.

GRANTS

This work was supported by NIH Grants 2R15 HL-129209-02 and 1R01 HL-116530 and Department of Veterans Affairs Merit Review Award BX001681.

DISCLOSURES

No conflicts of interest, financial or otherwise, are declared by the authors.

AUTHOR CONTRIBUTIONS

A.V.C. and S.H.A. conceived and designed research; K.B., B.M.R., and S.H.A. performed experiments; K.B., B.M.R., and S.H.A. analyzed data; A.V.C., E.R.J., and S.H.A. interpreted results of experiments; A.V.C. and K.B. prepared figures; A.V.C. drafted manuscript; A.V.C., K.B., B.M.R., and S.H.A. edited and revised manuscript; A.V.C., K.B., B.M.R., E.R.J., and S.H.A. approved final version of manuscript.

APPENDIX: DERIVATION OF GOVERNING DIFFERENTIAL EQUATIONS OF HMPAO PBPK MODEL

HMPAO lung uptake is given by the total of oxidized and reduced HMPAO in the pulmonary arteries, pulmonary capillary vascular and extravascular regions, and pulmonary veins. A model was developed to determine each of these components and hence the resulting lung TAC.

Single capillary element.

Each capillary element (Fig. 6) consists of a vascular region and a surrounding extravascular region, with volumes V_v and V_e, respectively. The model assumes the following:

•	**The lipophilic oxidized form of HMPAO can diffuse out of the vascular region into the extravascular region driven by concentration gradient.**
•	**Flow and hence convection are restricted to the vascular region.**
•	**Transport within the extravascular region occurs only by diffusion.**
•	**Instantaneous radial diffusion of both forms of HMPAO within the vascular and extravascular regions (Ref. 3).**
•	**Diffusion of both forms in the vascular and extravascular regions in the flow direction (*x*) is negligible compared with axial convective transport (Ref. 3).**
•	**The free (i.e., not albumin bound) oxidized form of HMPAO participates in rapidly equilibrating interactions with perfusate albumin (BSA) in the vascular region and with other proteins and/or binding sites in the extravascular region.**
•	**The free oxidized form of HMPAO is converted to the reduced form via a GSH-dependent and a GSH-independent process.**
•	**The GSH-dependent rate of HMPAO reduction in the vascular region is assumed to be zero.**
•	**Injected HMPAO is 100% in the oxidized form.**

Under these assumptions and using mass balance and laws of mass action, the temporal and spatial variations in the concentrations of the oxidized, $O(t,x)$, and reduced, $R(t,x)$, forms of HMPAO in the blood and tissue regions are described by the following PDEs:

$$\mathrm{V_v}\left(\frac{\partial O_\mathrm{B}}{\partial t} + W\frac{\partial O_\mathrm{B}}{\partial x}\right) = \mathrm{V_v}(k_{-1}O_\mathrm{v}P_\mathrm{v} - k_1 O_\mathrm{v}P_\mathrm{v}) + PS(O_\mathrm{e} - O_\mathrm{v}) \text{ (A1)}$$

$$\mathrm{V_v}\left(\frac{\partial O_\mathrm{v}P_\mathrm{v}}{\partial t} + W\frac{\partial O_\mathrm{v}P_\mathrm{v}}{\partial x}\right) = \mathrm{V_v}(k_1 O_\mathrm{v}P_\mathrm{v} - k_{-1}O_\mathrm{v}P_\mathrm{v}) \text{ (A2)}$$

$$\mathrm{V_e}\frac{\partial O_\mathrm{e}}{\partial t} = \mathrm{PS}(O_\mathrm{v} - O_\mathrm{e}) + \mathrm{V_e}(k_{-4}O_\mathrm{e}P_\mathrm{e} - k_4 O_\mathrm{e}P_\mathrm{e} - k_3 O_\mathrm{e}\mathrm{RH} - k_2 O_\mathrm{e}\mathrm{GSH}) \text{ (A3)}$$

$$\mathrm{V_e}\frac{\partial O_\mathrm{e}P_\mathrm{e}}{\partial t} = \mathrm{V_e}(k_4 O_\mathrm{e}P_\mathrm{e} - k_{-4}O_\mathrm{e}P_\mathrm{e}) \text{ (A4)}$$

$$\mathrm{V_e}\frac{\partial R_\mathrm{e}}{\partial t} = \mathrm{V_e}(k_3 O_\mathrm{e}\mathrm{RH} + k_2 O_\mathrm{e}\mathrm{GSH}) \text{ (A5)}$$

where $W = L/\mu_c$ is the average flow velocity within the capillary region and μ_c is the capillary mean transit time and $x = 0$ and $x = L$ are the capillary inlet and outlet, respectively. $O_v(x,t)$ and $O_e(x,t)$ are the respective vascular and extravascular concentrations of the oxidized form of HMPAO at distance *x* from the capillary inlet and time *t*. P_v and $P_B O_B(x,t)$ are the respective perfusate %BSA and vascular concentration of the BSA-bound form of oxidized HMPAO at *x* and *t*. P_e and $P_e O_e(x,t)$ are the respective concentrations of protein and protein-bound form of oxidized HMPAO within the extravascular region at *x* and *t*. GSH and RH are the concentrations of glutathione and other reductants, respectively, within the extravascular region.

Assuming rapidly equilibrating interactions between the oxidized form of HMPAO and albumin (BSA, P_v) in the vascular region, we obtain

$$k_{-1}O_\mathrm{v}P_\mathrm{v} = k_1 O_\mathrm{v}P_\mathrm{v} \text{ (A6)}$$

If we let $\bar{\mathrm{O}}_v = O_v + O_v P_v$ = total (free + bound) concentration of the oxidized form in V_v, then

$$\bar{O}_\mathrm{v} = O_\mathrm{v}\left(1 + \frac{P_\mathrm{v}}{K_\mathrm{Dv}}\right) \text{ (A7)}$$

where

$K_{Dv} = \frac{k_{-1}}{k_1}$ = equilibrium dissociation constant.

Similarly, assuming rapidly equilibrating interactions between oxidized HMPAO and proteins (P_e) in V_e, the total (free + bound) concentration of the oxidized form of HMPAO in V_e is given by

$$\bar{O}_e = O_e\left(1 + \frac{P_e}{K_{De}}\right) \text{ (A8)}$$

where

$K_{De} = \frac{k_{-4}}{k_4}$ = equilibrium dissociation constant.

Substituting *Eqs. A7* and *A8* into *Eqs. A1–A5* results in

$$\frac{\partial \bar{O}_v}{\partial t} + W\frac{\partial \bar{O}_v}{\partial x} = \frac{PS}{V_v}\left(\frac{\bar{O}_v}{1+\frac{P_v}{K_{Dv}}} - \frac{\bar{O}_e}{1+\frac{P_e}{K_{De}}}\right) \text{ (A9)}$$

$$\frac{\partial \bar{O}_e}{\partial t} = \frac{PS}{V_e}\left(\frac{\bar{O}_v}{1+\frac{P_v}{K_{Dv}}} - \frac{\bar{O}_e}{1+\frac{P_e}{K_{De}}}\right) - k_{GSH}\bar{O}_v - k_{RH}\bar{O}_v \text{ (A10)}$$

$$\frac{\partial R_e}{\partial t} = k_{GSH}\bar{O}_v + k_{RH}\bar{O}_v \text{ (A11)}$$

where

$$k_{GSH} = \frac{k_3}{1+\frac{P_e}{K_{De}}} \times \text{GSH and } k_{RH} = \frac{k_2}{1+\frac{P_e}{K_{De}}} \times \text{RH}$$

The boundary ($x = 0$) and initial ($t = 0$) conditions are then given by

$$\bar{O}_v(x,0) = \bar{O}_e(x,0) = R_e(x,0) = 0$$

$$\bar{O}_v(0,t) = C_{in}(t) \text{ and } \bar{O}_e(0,t) = R_e(0,t) = 0$$

where $C_{in}(t)$ is the capillary input function of the injected oxidized form of HMPAO.

Capillary bed.

The above PDEs (*Eqs. A9–A11*) are for a single capillary element. To account for the effect of capillary perfusion kinematics on the lung uptake of HMPAO, an organ model was used that accounts for the distribution of pulmonary capillary transit times, $h_c(t)$, and for the arterial and venous conducting vessels as previously described (3, 23). Briefly, the lung is assumed to consist of *N* parallel, noninteracting capillary elements, each with a different transit time t_i, $i = 1…N$ as shown in Fig. A1. Then $h_c(t)$ is the result of capillaries with different lengths, flows, cross-sectional areas, or any combination of these. However, the per-unit capillary vascular volume, exchange surface area, and physical and chemical properties are assumed to be the same for all capillary elements. Then let

$$H_i = \left(\frac{\Delta t}{2}\right)\left[h_c\left(t_i - \frac{\Delta t}{2}\right) + h_c\left(t_i + \frac{\Delta t}{2}\right)\right] \text{ (A12)}$$

$$\sum_{i=1}^{N} H_i = 1 \text{ (A13)}$$

where H_i is the flow-weighted fraction of capillaries with transit time t_i and Δt is the transit time increment. All capillaries are exposed to the same flow and capillary input function, $C_{in}(t)$, under the assumption of random coupling conditions between the conducting (i.e., arteries and veins) vessels and exchanging capillaries. For the

organ model, we assume no dispersion of the injected bolus in the conducting vessels so that the transit time distributions of the arteries and the veins are represented by shifted impulse functions (23).

To determine HMPAO in the capillaries, the governing PDEs above must be solved with the above initial and boundary conditions. A direct numerical approach is to first solve the resulting finite difference equations on each of the *N* capillaries, weight the output of each capillary by its corresponding H_i, and sum these weighted curves to obtain the concentrations of the oxidized form of HMPAO in the capillary vascular and extravascular regions at (*x*,*t*).

Because of the computational complexity of solving the system of PDEs on a distribution of capillaries, we used an alternative strategy for obtaining the concentrations at the outlet of the capillaries. The method involves solving the governing differential equations for a single capillary with the longest mean transit time and subsample from that result as previously described (3, 23) and briefly presented here. Without loss of generality, the spatial dimension can be normalized using *z = x/L* resulting in $\bar{O}_v(t,z)$, $\bar{O}_e(t,z)$, and $R_T(t,z)$. *Equation A9* for the capillary with the longest transit time t_N then becomes

$$\frac{\partial O_v}{\partial t}+\frac{1}{t_N}\frac{\partial O_v}{\partial z}=\frac{PS}{V_v}\left(\frac{\bar{O}_v}{1+\frac{P_v}{K_{Dv}}}-\frac{\bar{O}_e}{1+\frac{P_e}{K_{De}}}\right) \quad \text{(A14)}$$

with *Eqs. A10* and *A11* and the initial conditions interpreted accordingly. These PDEs are then solved at each Δ*t* and Δ*z* point using finite differences. Because the model produces a continuity wave that travels only in the positive *z* (axial) direction, the time-concentration functions at all *z* locations along this maximum mean transit time capillary can be interpreted as individual outflow concentration curves from capillaries with transit times corresponding to the *z* locations. This can be seen in Fig. A2, where the concentration at the *i*th node of the maximum transit time corresponds with the outflow concentration time curve for a capillary of transit time $t_i = i\Delta t$ (23).

Whole organ model.

HMPAO uptake is given by the total of oxidized and reduced HMPAO in the arteries, capillary vascular and extravascular regions, and veins. The lung input function, $C_{art}(t)$, was modeled as a shifted gamma variate function (18) with mean transit time μ, variance σ^2, and time shift t_0, i.e.,

$$C_{art}(t)=\begin{cases}0, t_0\le 0\\ (t-t_0)^{\left(\frac{\mu^2}{\sigma^2}\right)-1}\exp\left(-\frac{t-t_0}{(\sigma^2/\mu)}\right),\ t_0>0\end{cases}$$

Since no dispersion occurs within the conducting arteries, the input to the capillaries, $C_{in}(t)$, is a time-shifted version of $C_{art}(t)$. The capillary transit time distribution, $h_c(t)$, was also represented with a gamma variate function with mean transit time (μ_c) and variance (σ2cσc2) equal to previously measured values reported by Ramakrishna et al. (23). Similar to the arteries, transit through the veins is assumed to involve only a time shift (equal to the same as the arteries). Therefore output from the lung, $C_{vein}(t)$, is a time-shifted version of the capillary outflow curve. Finally, the model lung time-activity curve describing the total amount of ^{99m}Tc-HMPAO in the lung as a function of time, TAC(*t*), is the cumulative flow-weighted sum of the lung input concentration minus the output concentration at each time, i.e.,

$$TAC(t)=F\int_0^t[C_{art}(t)-C_{vein}(t)]\,dt$$

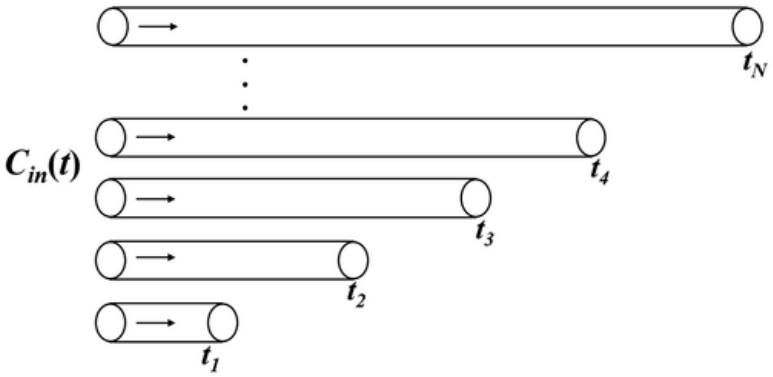

Fig. A1. *N* parallel pathways corresponding to *N* capillaries with different mean transit times (t_i, where *i* = 1, …, *N*). $C_{in}(t)$ is the capillary input function.

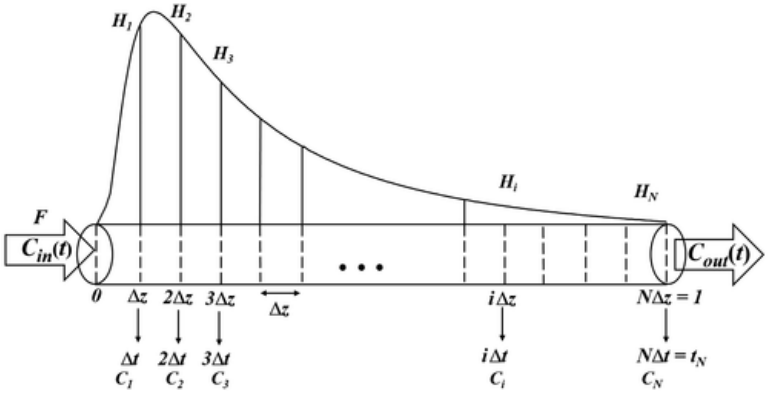

Fig. A2. Solution of the model partial differential equations for the capillary with the longest transit time. C_i corresponds to the outflow concentration for each capillary. H_i is the flow-weighted fraction of capillaries with transit time t_i. F, pump flow; *z*, distance from the capillary inlet; C_{in}, capillary input function; C_{out}, capillary output function.

AUTHOR NOTES

Address for reprint requests and other correspondence: A. V. Clough, Research Service 151, Milwaukee VA Medical Center, 5000 W. National Ave., Milwaukee, WI 53295 (e-mail: anne.clough@marquette.edu).

REFERENCES

1. Andersen AR. ^{99m}Tc-d,l-hexamethylene-propyleneamine oxime (^{99m}Tc-HMPAO): basic kinetic studies of a tracer of cerebral blood flow. ***Cerebrovasc Brain Metab Rev*** 1: 288–318, 1989.
2. Andersen AR, Friberg H, Lassen NA, Kristensen K, Neirinckx RD. Assessment of the arterial input curve for [^{99m}Tc]-d,l-HM-PAO by rapid octanol extraction. ***J Cereb Blood Flow Metab*** 8: S23–S30, 1988. doi:10.1038/jcbfm.1988.29.
3. Audi SH, Krenz GS, Linehan JH, Rickaby DA, Dawson CA. Pulmonary capillary transport function from flow-limited indicators. ***J Appl Physiol (1985)*** 77: 332–351, 1994. doi:10.1152/jappl.1994.77.1.332.
4. Audi SH, Roerig DL, Haworth ST, Clough AV. Role of glutathione in lung retention of ^{99m}Tc-hexamethylpropyleneamine oxime in two unique rat models of hyperoxic lung injury. ***J Appl Physiol (1985)*** 113: 658–665, 2012. doi:10.1152/japplphysiol.00441.2012.

5. Audi SH, Jacobs ER, Zhang X, Camara AK, Zhao M, Medhora MM, Rizzo B, Clough AV. Protection by inhaled hydrogen therapy in a rat model of acute lung injury can be tracked in vivo using molecular imaging. ***Shock*** 48: 467–476, 2017. doi:10.1097/SHK.0000000000000872.
6. Audi SH, Clough AV, Haworth ST, Medhora M, Ranji M, Densmore JC, Jacobs ER. 99mTc-hexamethylpropyleneamine oxime imaging for early detection of acute lung injury in rats exposed to hyperoxia or lipopolysaccharide treatment. ***Shock*** 46: 420–430, 2016. doi:10.1097/SHK.0000000000000605.
7. Bassingthwaighte JB, Chaloupka M. Sensitivity functions in the estimation of parameters of cellular exchange. ***Fed Proc*** 43: 181–184, 1984.
8. Bassingthwaighte JB, Raymond GM, Butterworth E, Alessio A, Caldwell JH. Multiscale modeling of metabolism, flows, and exchanges in heterogeneous organs. ***Ann NY Acad Sci*** 1188: 111–120, 2010. doi:10.1111/j.1749-6632.2009.05090.x.
9. Beard DA, Bassingthwaighte JB, Greene AS. Computational modeling of physiological systems. ***Physiol Genomics*** 23: 1–3, 2005. doi:10.1152/physiolgenomics.00117.2005.
10. Clough AV, Audi SH, Haworth ST, Roerig DL. Differential lung uptake of ^{99m}Tc-hexamethylpropyleneamine oxime and ^{99m}Tc-duramycin in the chronic hyperoxia rat model. ***J Nucl Med*** 53: 1984–1991, 2012. doi:10.2967/jnumed.112.108498.
11. Dawson CA, Roerig DL, Rickaby DA, Nelin LD, Linehan JH, Krenz GS. Use of diazepam for interpreting changes in extravascular lung water. ***J Appl Physiol (1985)*** 72: 686–693, 1992. doi:10.1152/jappl.1992.72.2.686.
12. Gumuser G, Vural K, Varol T, Parlak Y, Tuglu I, Topal G, Sayit E. Assessment of lung toxicity caused by bleomycin and amiodarone by Tc-99m HMPAO lung scintigraphy in rats. ***Ann Nucl Med*** 27: 592–599, 2013. doi:10.1007/s12149-013-0722-8.
13. Hang LW, Shiau YC, Hsu WH, Tsai JJ, Yeh JJ, Kao A. Increased lung uptake of technetium-99m hexamethylpropylene amine oxime in diffuse infiltrative lung disease. ***Respiration*** 70: 479–483, 2003. doi:10.1159/000074203.
14. Karau KL, Molthen RC, Dhyani A, Haworth ST, Hanger CC, Roerig DL, Johnson RH, Dawson CA. Pulmonary arterial morphometry from microfocal X-ray computed tomography. ***Am J Physiol Heart Circ Physiol*** 281: H2747–H2756, 2001. doi:10.1152/ajpheart.2001.281.6.H2747.
15. Kelm RF, Wagenführer J, Schmidtmann I, Engelhard K, Werner C, Noppens RR. Transpulmonary cardiac output measurement in a rat model of cardiac arrest and CPR: impact of vascular access. ***Resuscitation*** 81: 248–254, 2010. doi:10.1016/j.resuscitation.2009.10.024.
16. Knickelbein RG, Ingbar DH, Seres T, Snow K, Johnston RB Jr, Fayemi O, Gumkowski F, Jamieson JD, Warshaw JB. Hyperoxia enhances expression of gamma-glutamyl transpeptidase and increases protein *S*-glutathiolation in rat lung. ***Am J Physiol Lung Cell Mol Physiol*** 270: L115–L122, 1996. doi:10.1152/ajplung.1996.270.1.L115.
17. Lassen NA, Andersen AR, Friberg L, Paulson OB. The retention of [^{99m}Tc]-*d*,*l*-HM-PAO in the human brain after intracarotid bolus injection: a kinetic analysis. ***J Cereb Blood Flow Metab*** 8: S13–S22, 1988. doi:10.1038/jcbfm.1988.28.
18. Madsen MT. A simplified formulation of the gamma variate function. ***Phys Med Biol*** 37: 1597–1600, 1992. doi:10.1088/0031-9155/37/7/010.
19. Matsuda H, Oba H, Seki H, Higashi S, Sumiya H, Tsuji S, Terada H, Imai K, Shiba K, Mori H, Hisada K. Determination of flow and rate constants in a kinetic model of [^{99m}Tc]-hexamethyl-propylene amine oxime in the human brain. ***J Cereb Blood Flow Metab*** 8: S61–S68, 1988. doi:10.1038/jcbfm.1988.34.
20. Neirinckx RD, Burke JF, Harrison RC, Forster AM, Andersen AR, Lassen NA. The retention mechanism of technetium-99m-HM-PAO: intracellular reaction with glutathione. ***J Cereb Blood Flow Metab*** 8: S4–S12, 1988. doi:10.1038/jcbfm.1988.27.
21. Pacht ER, Timerman AP, Lykens MG, Merola AJ. Deficiency of alveolar fluid glutathione in patients with sepsis and the adult respiratory distress syndrome. ***Chest*** 100: 1397–1403, 1991. doi:10.1378/chest.100.5.1397.

22. Ragaller M, Richter T. Acute lung injury and acute respiratory distress syndrome. ***J Emerg Trauma Shock*** 3: 43–51, 2010. doi:10.4103/0974-2700.58663.
23. Ramakrishna M, Gan Z, Clough AV, Molthen RC, Roerig DL, Audi SH. Distribution of capillary transit times in isolated lungs of oxygen-tolerant rats. ***Ann Biomed Eng*** 38: 3449–3465, 2010. doi:10.1007/s10439-010-0092-5.
24. Schroeder T, Vidal Melo MF, Musch G, Harris RS, Venegas JG, Winkler T. Image-derived input function for assessment of ^{18}F-FDG uptake by the inflamed lung. ***J Nucl Med*** 48: 1889–1896, 2007. doi:10.2967/jnumed.107.041079.
25. Suga K, Uchisako H, Nishigauchi K, Shimizu K, Kume N, Yamada N, Nakanishi T. Technetium-99m-HMPAO as a marker of chemical and irradiation lung injury: experimental and clinical investigations. ***J Nucl Med*** 35: 1520–1527, 1994.